JOURNAL OF AGRICULTURAL AND FOOD CHEMISTRY

J. Agric. Food Chem. **2006,** *54,* 5769–5776 **5769**

Chromoplast Morphology and β-Carotene Accumulation during Postharvest Ripening of Mango Cv. 'Tommy Atkins'

ANA LUCÍA VÁSQUEZ-CAICEDO,[‡,#] ANNEROSE HELLER,[§] SYBILLE NEIDHART,*[,‡] AND REINHOLD CARLE[‡]

Institute of Food Technology, Section Plant Foodstuff Technology, Hohenheim University, August-von-Hartmann-Strasse 3, 70599 Stuttgart, Germany, and Institute of Botany, Hohenheim University, Garbenstrasse 30, 70599 Stuttgart, Germany

Accumulation of β-carotene and *trans*−*cis* isomerization of ripening mango mesocarp were investigated as to concomitant ultrastructural changes. Proceeding postharvest ripening was shown by relevant starch degradation, tissue softening, and a rising sugar/acid ratio, resulting in a linear decrease ($R^2 = 0.89$) of a ripening index (RPI_{KS}) with increasing ripening time. A modest accumulation of all-*trans*-β-carotene and its *cis* isomers resulted in a slight pigmentation of the mango chromoplasts, because ambient temperatures of 18.2−19.5 °C provided suboptimal ripening conditions, affecting color development and β-carotene biosynthesis. The ultrastructures of chromoplasts from mango mesocarp and carrot roots were comparatively studied by means of light and transmission electron microscopy. Irrespective of the ripening stage, mango chromoplasts showed numerous plastoglobuli varying in size and electron density. They comprised the main part of carotenoids, thus supporting the partial solubilization of the pigments in lipid droplets. However, because different pigment-carrying tubular membrane structures were also observed, mango chromoplasts were assigned to the globular and reticulotubular types, whereas the crystalline type was confirmed for carrot chromoplasts. The large portions of naturally occurring *cis*-β-carotene in mango fruits contrasted with the predominance of the all-*trans* isomer characteristic of carrots, indicating that the nature of the structure where carotenoids are deposited and the physical state of the pigments are crucial for the stability of the all-*trans* configuration.

KEYWORDS: **β-Carotene stereoisomers; chromoplast ultrastructure; electron microscopy; *Mangifera indica* L.; postharvest ripening**

INTRODUCTION

As β-carotene accounts for more than half of the total carotenoid content in most cultivars, the mango fruit (*Mangifera indica* L.) substantially contributes to provitamin A supply in tropical and subtropical countries (*1*). Fruit development involves a maturation phase consisting of initial cell division, followed by a period of cell growth and increase in size of laticiferous canals and intercellular spaces, until a maximum organ expansion is reached (*2*, *3*). During the subsequent ripening phase, several metabolic changes influence the chemical composition and structural characteristics of the fruit (*3*, *4*). Among these changes, accumulation of β-carotene in mango fruits has been previously emphasized in terms of interrelationships with mesocarp color and resulting vitamin A values (*1*). Understanding of the concomitant morphological changes of the structures where these pigments are deposited during maturation and postharvest ripening is expected to provide a deeper insight into the nature and availability of carotenoids and, hence, the nutritional and sensory quality of mango fruits.

During fruit development, the growth phase of the cell generally concurs with plastid division, with structural and biochemical changes yielding several interconvertible plastid types of specialized functions (*5*). In capsicum fruits, early ripening stages are characterized by the presence of chloroplasts (*6*), where carotenoids are part of the pigment−protein complex of the photosystems I and II in the stroma- and grana-thylakoids. During fruit ripening, chloroplasts differentiate into chromoplasts by disintegration of the thylakoid membranes and by the development of new pigment-bearing structures (*6*). The latter is also marked by biochemical changes such as degradation of chlorophyll and pigment-associated proteins as well as the accumulation of carotenoids and chromoplast-specific proteins (*7*), as observed in pepper (*Capsicum annuum* L.) (*6*) and tomato (*Lycopersicon esculentum* L.) (*8*).

* Corresponding author [telephone +49(0)711 459 2317; fax +49(0)-711 459 4110; e-mail neidhasy@uni-hohenheim.de].

‡ Institute of Food Technology.

Present address: National Nutrition Survey II, Federal Research Centre for Nutrition and Food (BfEL), Location Karlsruhe, Haid-und-Neu-Strasse 9, 76131 Karlsruhe, Germany.

§ Institute of Botany.

10.1021/jf060747u CCC: $33.50
Published on Web 07/13/2006

Chromoplasts mostly occur in mature tissues and are generally classified as globular, tubular, reticulotubular, membranous, and crystalline types (*9*). The carotenoids may differ in their physical properties and bioavailability according to the underlying chromoplast structure. For instance, crystalline bodies have been observed in carrots (*10*) and tomatoes (*11*), where the thermodynamically more stable all-*trans* configurations of carotene and lycopene, respectively, are predominant. Consistently, the *cis* isomers of α- and *β*-carotene are usually missing in fresh carrot roots or are found in only minor amounts (*12*, *13*), leading to the assumption that the crystalline structure of the chromoplast is enhancing the stability of the all-*trans* configuration. This is supported by the detection of *cis* isomers in carrots after heat treatment and attributed to the fact that carotenes partly dissolve in cellular lipids as chromoplasts disintegrate during heating (*12*). However, although the conversion rate of the all-*trans* isomers into retinal is higher and the latter are more readily absorbed than their *cis*-isomeric forms, absorption of all-*trans*-α- and *β*-carotene is affected by their crystalline structure in carrots, resulting in poor bioavailability (*14*).

As opposed to carrot roots, large amounts of naturally occurring *cis*-*β*-carotene isomers have been reported in mangoes and several other fruits (*1*, *15*), indicating their deposition in chromoplast substructures other than crystalline types. Moreover, the large portion of *cis*-*β*-carotene isomers found in fresh mango mesocarp tissues has been assumed to be due to partial solubilization of *β*-carotene in lipid globules (*1*, *14*). This would occur in the globular chromoplast type, where carotene-carrying lipid droplets or plastoglobuli are found (*9*). However, to validate this assumption, the chromoplast ultrastructure in mango mesocarp tissues remained to be elucidated.

Therefore, the objective of the present work was to identify the type of chromoplasts present in the mango fruit mesocarp. To explain differences in the physical state and stability of *β*-carotene from different plant origins, carrot chromoplasts were included in this study. Furthermore, changes in mango chromoplast structures during fruit ripening were evaluated, as an attempt to explain the accumulation of *cis*-*β*-carotene at early ripening stages.

MATERIALS AND METHODS

Materials and Reagents. Fresh mango fruits of cv. 'Tommy Atkins' at their mature green-ripe stage and fresh carrot roots of cv. 'Napoli' were obtained from the wholesale market in Stuttgart, Germany. All reagents and solvents were of analytical or HPLC grade (VWR, Darmstadt, Germany). all-*trans*-*β*-Carotene (type II, HPLC purity > 95%; Sigma, St. Louis, MO) and *trans*-*β*-apo-8′-carotenal (purity ∼ 98% UV; Fluka, Buchs, Switzerland) were used for external calibration and as internal standard, respectively.

Mango Sample Collection. Approximately 30 kg of mangoes at their mature green-ripe stage was ripened for 8 days at 18.2−19.5 °C and a relative humidity of 73.6−77.6%. For chromoplast characterization by electron microscopy, three mango fruits per sampling date were randomly collected after 0, 2, and 7 days of ripening and investigated individually. Mesocarp tissue was obtained from the central portion of each mango half, at a distance of ∼2 cm from the peel. Furthermore, the mesocarp of each fruit was characterized by physicochemical ripeness analyses (color, firmness, pH, total soluble solids, titratable acidity) and its *β*-carotene content. Total soluble solids, titratable acidity, pH, and firmness were additionally determined using a pooled mesocarp sample that comprised the three mangoes at equal parts. Progress in postharvest ripening was monitored by sampling after 1, 3, 4, 6, and 8 days of ripening and subsequent physicochemical ripeness analyses based on the parameters mentioned above. For this purpose, five mango fruits were randomly collected, peeled, pitted, cut into pieces of 1−2 cm^3, and pooled. From the pooled sample, an aliquot of ∼250−300 g was used for texture measurements, whereas the rest was ground in a laboratory mixer of the type Grindomix GM 200 (Retsch, Haan, Germany) for the analyses of the other parameters.

Carrot Sample Collection. Approximately 20 kg of fresh carrot roots was stored together with the mango fruits for 8 days at 18.2−19.5 °C and a relative humidity of 73.6−77.6%. By analogy with mangoes, carrot samples constituting the controls in chromoplast investigations were equally collected after 0, 2, and 7 days of storage. Carrot tissue was obtained from the cortex of a randomly selected carrot root, at a distance of ∼2 cm from the periderm.

Chemical Analyses. Homogenized fresh mango mesocarp was used for immediate determination of total soluble solids (TSS), titratable acidity (TA), and pH (*16*), whereas an aliquot was packed into aluminum pouches, sealed under vacuum, and stored at −80 °C until *β*-carotene analysis. TSS was measured refractometrically using a digital refractometer of the type RX 5000 (Atago, Tokyo, Japan). For measurements of pH, a pH-meter microprocessor of the type pH 535 MultiCal (WTW, Weilheim, Germany) was employed. By the use of an automatic titration system of the type Titrino 718 STAT (Deutsche Metrohm, Filderstadt, Germany), TA was determined by titration with 0.1 N NaOH to a pH of 8.1 and expressed as citric acid in grams per 100 g.

Texture Analyses. Firmness of mango mesocarp was measured by application of an Instron Universal Texture Analyzer (series IX 4301; Instron Deutschland, Darmstadt, Germany) equipped with a Kramer shear cell. Tissues were cut into cubes of ∼1 cm^3. For each measurement, an aliquot of ∼30 g was exactly weighed and evenly distributed to form a single layer in the Kramer shear cell. Three to seven measurements were carried out per sample, depending on the amount of material available. Results were expressed as the specific maximum load ($SF_{KS,i}$ in N/100 g, where the label "KS" is assigned to the underlying mode of texture analysis based on the Kramer shear cell) by relating the observed maximal shear load ($F_{KS,i}$ in N) to the sample fresh weight examined.

Ripening Index. Similar to previous studies (*1*, *17*), postharvest ripeness of the mango fruits was quantitatively described by a ripening index (RPI_{KS}) calculated according to eq 1, where the dimensionless

$$RPI_{KS} = \ln(100 \cdot SF_{KS} \cdot TSS^{-1} \cdot TA) \quad (1)$$

fruit firmness ($SF_{KS} = |SF_{KS,i}|$) refers to the absolute value of the specific maximum load at the ripening time RT_i (in days) and TSS/TA specifies the sugar/acid ratio of the corresponding mango mesocarp sample that was calculated from TSS and TA.

Color Measurements. As detailed elsewhere (*1*), the color of mango mesocarp was evaluated using a freshly obtained purée. For each sample, color data sets were measured 6-fold with a colorimeter CR300 (Minolta, Langenhagen, Germany) based on the CIELAB color system (L^*, a^*, b^* and L^*, C^*, $H°$, respectively).

***β*-Carotene Analyses.** Frozen mango mesocarp samples were quickly thawed in their pouches at 20 °C in a water bath. Approximately 10 g of an exactly weighed sample was homogenized for 10−20 s by the use of an Ultra-turrax (Janke & Kunkel, Stauffen, Germany). Subsequently, *β*-carotene was extracted as described by Vásquez-Caicedo et al. (*1*) and determined by HPLC on a C_{30}-phase, according to the method of Marx et al. (*18*), with a Shimadzu system consisting of an autoinjector SIL-10ADvp, a system controller SCL-10Avp, a pump FCV-10ALvp, a solvent delivery module LC-10ATvp, a degasser GT 154, a column oven CTO-10ALvp, and a diode array detector SPD-M10Avp (Shimadzu, Kyoto, Japan). Quantification of all-*trans*-*β*-carotene at 453 nm was based on a linear calibration curve, as previously reported (*1*). By analogy, 9-*cis*- and 13-*cis*-*β*-carotene isomers were monitored at 445 nm, calculating their concentrations from a respective all-*trans*-*β*-carotene calibration curve. At least five standard concentrations were used for each calibration curve that ranged from 0.5 to 19.9 mg/L for all-*trans*-*β*-carotene and from 0.25 to 2.5 mg/L for the *cis*-*β*-carotene isomers. In addition to the total *β*-carotene content, the vitamin A value was finally calculated from the observed *β*-carotene isomer contents on the basis of the FAO/WHO guidelines (*19*) for *β*-carotene from mixed meal and the relative bioconversion of the *cis* isomers described by Zechmeister (*20*) to assess the effects of

Table 1. Mango Fruit Quality before (Mature Green-Ripe Stage) and after Postharvest Ripening until Full Ripeness[a]

RT (days)	TSS/TA	RPI_{KS}	$H°$	C^*	β-carotene (μg/100 g of DW) all-*trans*	13-*cis*	9-*cis*	total *cis* isomers (%)	vitamin A[b] (RE/100 g of DW)
0	17.5	10.34	91.8 ± 0.2	50.5 ± 0.6	1798 ± 111	264 ± 5	58 ± 19	15.2	327[c] ± 20
8	51.9	7.35	93.4 ± 0.0	48.9 ± 0.2	1970 ± 7	312 ± 2	237 ± 2	21.8	371[d] ± 1

[a] Determined by analysis of pooled samples as far as available. Otherwise, average values obtained from analyses of individual fruits per ripening day (RT) are indicated. [b] Retinol equivalents (RE) calculated from the contents of all-*trans*- (C_{AT}), 13-*cis*- (C_{13-cis}), and 9-*cis*-β-carotene (C_{9-cis}) in μg/100 g of dry weight (DW) on the basis of the bioconversion rate concluded by the FAO/WHO Joint Expert Consultation (*19*) for all-*trans*-β-carotene from a mixed meal and the relative bioconversion of the *cis* isomers according to Zechmeister (*20*): vitamin A value = $(6^{-1}C_{AT}) + 0.53\ (6^{-1}C_{13-cis}) + 0.38\ (6^{-1}C_{9-cis})$. [c] Corresponding retinol activity equivalents (*21*): 163 RAE/100 g of DW. [d] Corresponding retinol activity equivalents (*21*): 187 RAE/100 g of DW.

the *cis*-isomer levels at different ripening stages, irrespective of the fact that the assumed equivalency of 6 μg of all-*trans*-β-carotene to 1 μg of retinol may result in overestimation of the vitamin A activity (*21*−*23*). By comparison with previous studies on carotenoid profiles of mango fruits (*1*, *15*, *24*), vitamin A values calculated by analogy allowed the overall quality of the fruit samples studied to be ranked. According to the revised estimates of the Institute of Medicine (IOM) of the U.S. National Academy of Sciences (*21*), 12 μg of all-*trans*-β-carotene and 24 μg of other provitamin A carotenoids, respectively, have the same activity as 1 μg of retinol. However, the bioefficacy of β-carotene may be even lower (*22*, *23*). In view of the current discussion on the bioefficacy of carotenoids (*23*), retinol activity equivalents (RAE) according to the IOM guidelines (*21*) were additionally indicated, whereas the main focus was on the contents of the β-carotene isomers. The latter as well as the vitamin A values were indicated on a dry weight (DW) basis. To determine mesocarp dry matter, the water content of an exactly weighed homogenized sample of ∼0.05 g was quantified by Karl Fischer titration in a one-component system at 50 °C (*25*), using a Titrino 718 (Deutsche Metrohm, Filderstadt, Germany) in the 'SET Ipol' mode for set-endpoint titration controlled by a preset polarization current.

Microscopic Studies. For transmission electron microscopy, sections of mango mesocarp (0.5 mm × 2.0 mm^2) were obtained from the inner part of the fruit at a distance of ∼2 cm from the peel by the use of a razor blade. Similarly, samples were taken from the cortex of carrot roots to compare chromoplast morphology. The samples were fixed with glutaraldehyde (c = 2.5%) in 0.1 M sodium phosphate buffer (pH 7.2) for 1 h at room temperature. After three washing steps with sodium phosphate buffer, postfixation was performed with osmium tetroxide (c = 1%) in the same buffer for 1 h. Subsequently, the samples were washed three times with redistilled water and dehydrated in a series of acetone prior to embedding in Epon and polymerization at 60 °C. Using an Ultracut UCT microtome (Leica, Wetzlar, Germany), ultrathin sections were cut with a diamond knife, collected on pioloform-carbon-coated copper grids, and stained with uranyl acetate and lead citrate prior to examination in a Zeiss EM 10 transmission electron microscope (Oberkochen, Germany) at 60−80 kV.

For light microscopy, fresh, free-hand sections of the corresponding mango and carrot tissue were cut with glass knives, mounted on glass slides, stained with an aqueous toluidine blue solution (c = 0.5%), and examined with a Zeiss Axioplan light microscope (Göttingen, Germany) coupled to a Leica DC 200 digital camera (Wetzlar, Germany) for image recording. Further sections without that kind of staining were also examined. For the latter, a classical iodine−starch staining solution was used to identify starch in mango mesocarp tissues (*26*).

RESULTS

Quality Changes of Mango Fruits during Postharvest Ripening. Postharvest ripening was characterized by a weak increase of TSS and a notable decline of TA after the second day (**Figure 1A**). This was in contrast with previous findings (*27*), where TSS approached a constant level after a considerable increase during the first 2−3 days of ripening. Accordingly, ripening of the mango fruits was retarded at ambient temperatures of 18.2−19.5 °C, as shown by irrelevant variations of

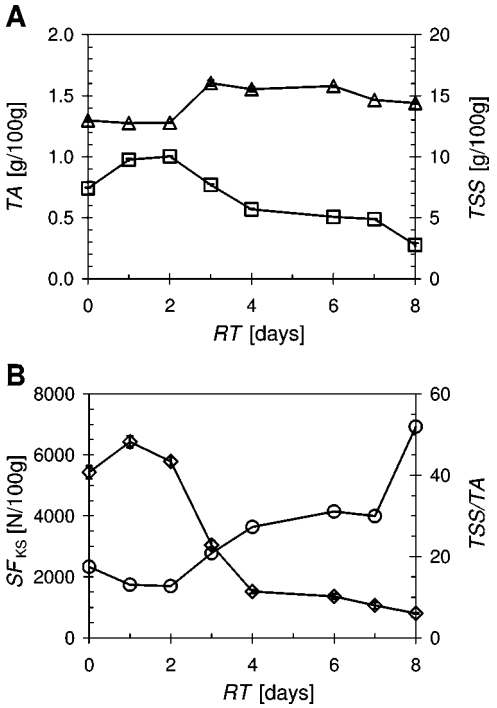

Figure 1. Changes in mesocarp characteristics during postharvest ripening of cv. 'Tommy Atkins' mangoes at 18.2–19.5 °C: (**A**) titratable acidity (□, TA) and total soluble solids (△, TSS); (**B**) firmness (◇, SF_{KS}) and sugar/acid ratio (○, TSS/TA). RT, ripening time.

the sugar/acid ratio (TSS/TA) and mesocarp firmness during the first 2 days (**Figure 1B**). This initial lag phase was followed by a slow increase of TSS/TA up to day 7 and a sharp rise at day 8. The overall rise in TSS/TA by 34.4 units (197%) was reflected by the marginal overall increase in total soluble solids by 11.0% that was accompanied by a considerable total loss of titratable acidity by 62.6% and a slight increase in pH by 0.4 unit after 8 days of ripening.

On the other hand, firmness strongly declined between days 2 and 4, followed by minor softening until day 8, finally resulting in an overall loss of firmness by 85%. Despite the delayed onset of the ripening process and the irregular kinetic differences between subsequent progress of softening and development of TSS/TA, the ripening index (RPI_{KS}) calculated from mesocarp firmness and TSS/TA of the pooled samples (eq 1) linearly decreased with proceeding ripening time (RT) (**Figure 2A**). Observed linearity was based on a coefficient of determination of R^2 = 0.89. The linear behavior was consistent with the function proposed in previous studies (*1*, *17*) to describe the dependence of an analogous ripening index on RT. Thus, the suitability of the ripening index as an unambiguous tool for mathematical modeling of postharvest ripening changes in mango fruits was confirmed.

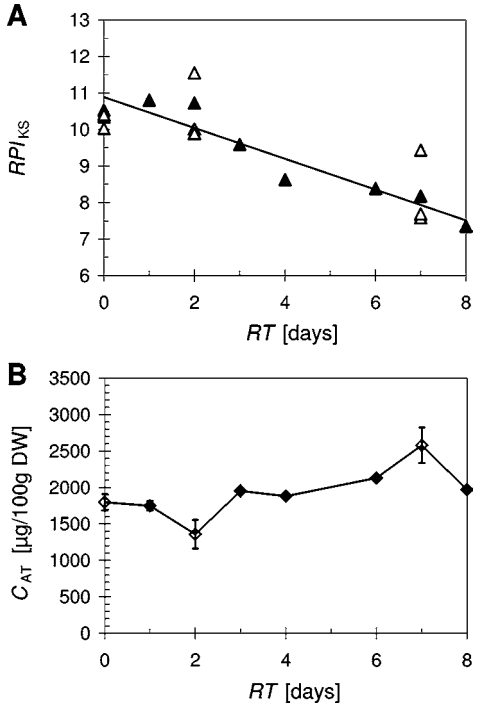

Figure 2. Postharvest carotenogenesis of cv. 'Tommy Atkins' mangoes ripened at 18.2–19.5 °C: (**A**) postharvest ripening index (RPI_{KS}, triangles) as a linear function of ripening time (RT), calculated from data sets of pooled samples ($R^2 = 0.89$); (**B**) development of all-*trans*-β-carotene contents (C_{AT}, rhombs). (▲, ◆) RPI_{KS} and C_{AT} of pooled samples, respectively; (△) RPI_{KS} of fruits individually analyzed; (◇) average C_{AT} from fruits individually analyzed; DW, dry weight.

After 8 days of ripening, the mango fruits hardly displayed a color shift (**Table 1**). As shown by hue angles ($H°$) of 91.8−93.4°, a rather pure yellow mesocarp color was largely retained. In accordance with the minor color changes of the mesocarp, no interrelationships between RPI_{KS} and hue ($H°$) or chroma (C^*) were detectable by regression analyses in this study (data not shown), unlike previous reports on mango fruits displaying marked cultivar-specific color changes when the monitoring of postharvest ripening at subtropical climatic conditions was started immediately after harvest (*1*). Similarly, only marginal accumulation of all-*trans*-β-carotene (C_{AT}) was observed with rising postharvest time (RT) (**Figure 2B**). Due to minor changes of C_{AT} and concomitant heterogeneity of the fruits studied, the C_{AT}−RT data sets allowed no modeling by adequate regression, unlike previous findings for fruits of various cultivars with significant postharvest β-carotene accumulation (*1*). Consistently, all-*trans*-β-carotene increased by only 9.6% throughout the observation period of 8 days, whereas 13-*cis*-β-carotene showed an overall rise by 18.2% (**Table 1**). Surprisingly, 9-*cis*-β-carotene rose to a 4-fold level during ripening, resulting in final isomer portions of 78.2, 12.4, and 9.4% for all-*trans*-, 13-*cis*-, and 9-*cis*-β-carotene, respectively. On the whole, total β-carotene increased by 18.9%. **Table 1** summarizes the most relevant quality characteristics of the fruits at their mature-green stage (day 0) and at full ripeness (day 8).

In the end, postharvest ripening of the fruit batch studied veritably proceeded, but with notable variations among the fruits (**Figure 2A**) and only marginal pigment formation under the prevailing circumstances.

Morphology of Mango Chromoplasts. In mango fruit tissue, chromoplasts occurred at all ripening stages studied and not only in the mesophyll cells but also in the tissue of the vascular bundle. Softening of the cell wall, enlargement of vacuoles, and

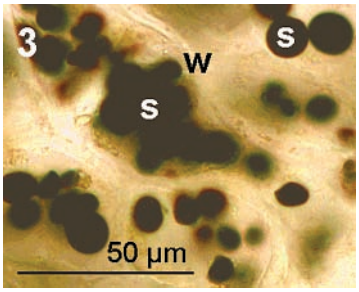

Figure 3. Light micrograph of starch grains (s) in the chromoplasts of unripe mango mesocarp cells (ripening day 0) stained with an iodine–starch indicator. (w) compact cell wall.

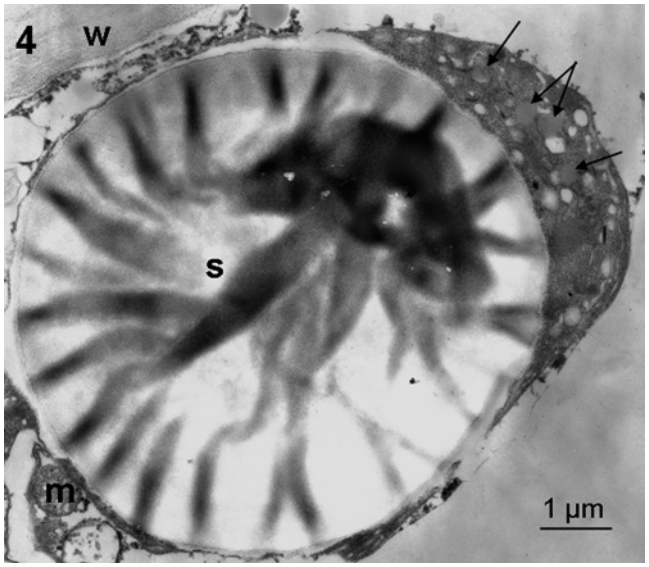

Figure 4. Transmission electron micrograph of a chromoplast with a large starch grain (s) of an unripe mango mesophyll cell (ripening day 0). (Arrows) pigment containing plastoglobuli; (w) cell wall; (m) mitochondrium.

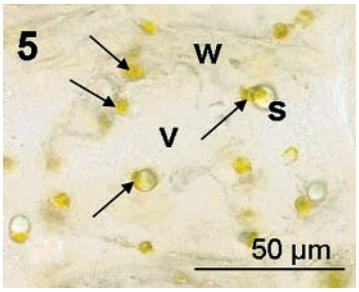

Figure 5. Light micrograph of a ripe mango mesophyll cell (ripening day 7) without any staining showing the typical color of mango chromoplasts (arrows). Some starch grains (s) are still visible. The ripe mesophyll cell shows a "soft cell wall" (w) and an enlarged vacuole (v).

starch grains decreasing in number and size were signs of the ripening process. In unripe fruits, plastids of fruit mesophyll cells were dominated by large starch grains (**Figures 3** and **4**), but they had already developed into chromoplasts. Therefore, the differentiation into chromoplasts had occurred at an earlier stage of the fruit development. During fruit ripening, the number and size of starch grains decreased (**Figure 5**), whereas numerous large plastoglobuli were present in the chromoplasts of fruit mesophyll cells, irrespective of the ripening stage (**Figures 4**−**8**). The size of the plastoglobuli in the fruit mesophyll cells varied with diameters from 0.1 to 0.5 μm. In the generally smaller vascular parenchyma cells, the plastoglo-

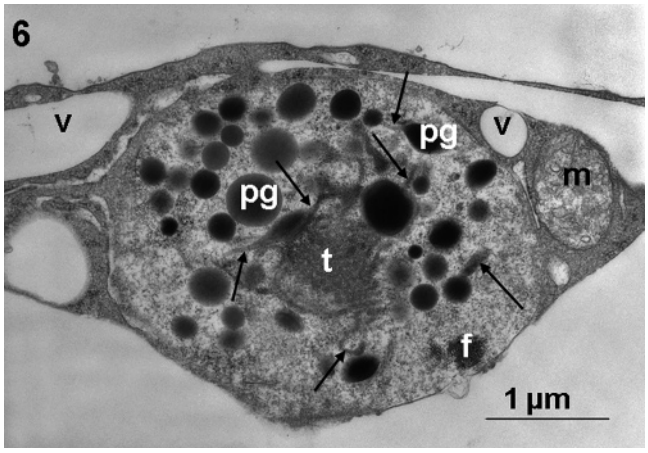

Figure 6. Transmission electron micrograph of the chromoplasts of a ripe mango mesophyll cell (ripening day 7) with numerous pigment-containing plastoglobuli (pg) of varying size and electron density, single tubular membranes (arrows), and a network of tubular membranes with electron-dense contents (t), crystalline phytoferritin (f), vacuole (v), and mitochondrium (m).

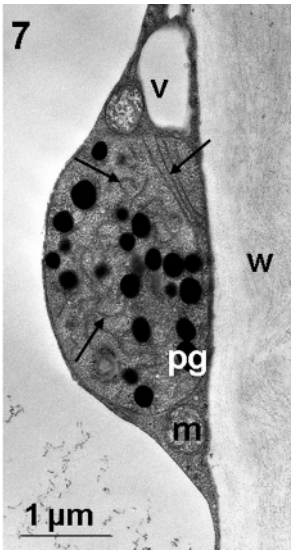

Figure 7. Transmission electron micrograph of chromoplasts of a ripe mango mesophyll cell (ripening day 7) with plastoglobuli (pg), stroma thylakoids (arrows), mitochondrium (m), vacuole (v), and cell wall (w).

buli were also smaller (0.08−0.17 μm). In addition to the plastoglobuli, tubular membranes with and without electron-dense contents were observed as single tubules and as characteristic networks (**Figures 6** and **9**). Elongated forms of plastoglobuli and their connection to membranes could be assumed as developing stages (**Figures 6** and **8**). Single stroma thylakoids, individual prolamellar-like bodies (**Figures 7** and **8**, respectively), and crystalline structures (**Figure 6**), which might represent phytoferritin, could be detected. On the basis of the latter observations and the classification of chromoplasts suggested by Sitte et al. (*9*), mango chromoplasts are a combination of the globular and reticulotubular type.

Morphology of Carrot Chromoplasts. In contrast to mango, carrot chromoplasts belong to the crystalline type. Carrot chromoplasts contained long, often needle-shaped carotene crystals (**Figures 10** and **11**), which were located inside membrane-surrounded compartments, as clearly shown elsewhere (*9*, *10*). The crystals dictated the shape of the chromoplasts, as they could grow to light-microscopic dimensions

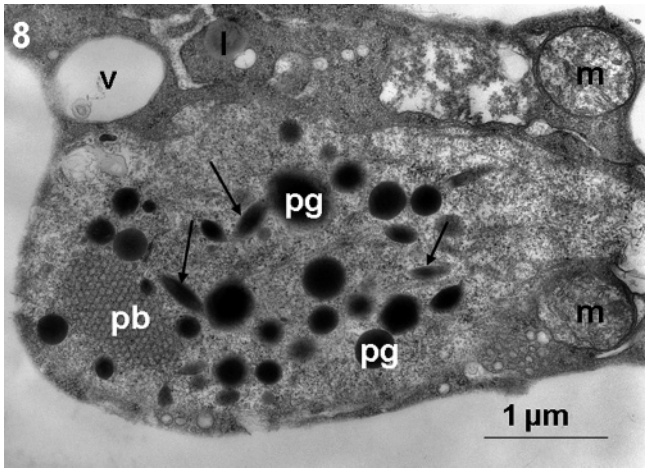

Figure 8. Chromoplasts of a ripe mango mesophyll cell (ripening day 7) with globuli (pg) and developing plastoglobuli (arrows). Transmission electron micrograph with prolamellar-like body (pb), lipid body (l), mitochrondrium (m), and vacuole (v).

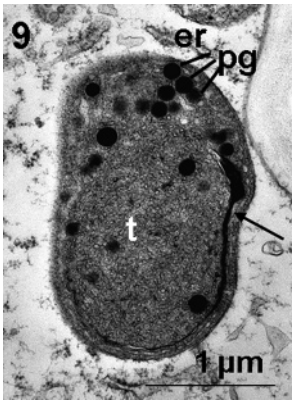

Figure 9. Transmission electron micrograph of a small chromoplast in a vascular parenchyma cell from ripe mango (ripening day 7) with small plastoglobuli (pg), a network of tubular membranes (t), and a single membrane cisterna with electron-dense content (arrow). (er) endoplasmatic reticulum.

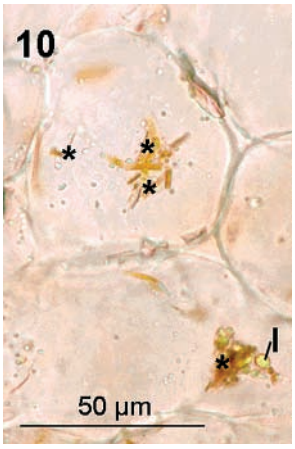

Figure 10. Light micrograph of cortex cells of carrot root showing typical color and structure of the crystalline type of chromoplasts (asterisks). (l) lipid body.

and gave rise to unusually formed chromoplasts. Plastoglobuli of carrots were much smaller (<0.1 μm in diameter) compared to mango plastoglobuli. Furthermore, individual thylakoids and single starch grains were observed in carrot chromoplasts.

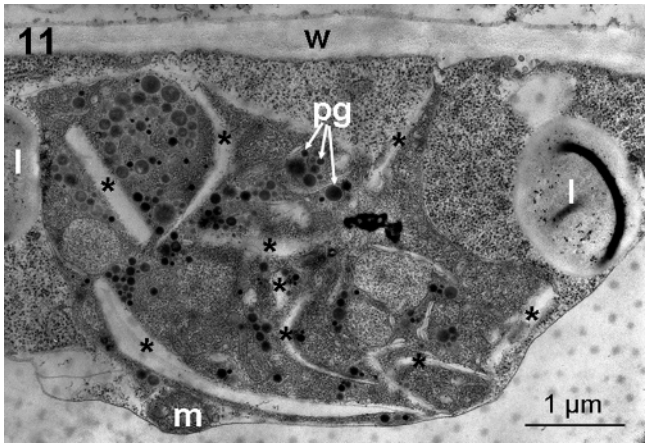

Figure 11. Transmission electron micrograph of a chromoplast of the crystalline type in carrot root tissue. (Asterisks) crystals, carotene extracted; (pg) small plastoglobuli; (l) lipid body; (m) mitochondrium; (w) cell wall.

DISCUSSION

The development of a yellow-orange coloration during postharvest ripening of most mango cultivars results from the accumulation of carotenoids in the mesocarp tissue, concurrent with a decreasing ripening index (*1*). The poor color development and concomitant low β-carotene content observed in this study led to the assumption that these results were partly cultivar-specific. However, in comparison with the present study, 1.8-fold levels of all-*trans*-β-carotene were reported for cv. 'Tommy Atkins' mangoes ripened at ~30 °C (*15*). Therefore, it could be inferred that the temperatures of 18.2−19.5 °C controlling postharvest ripening probably retarded metabolic processes, as discussed by other authors (*28*). Although the temperatures applied fell in the optimum range recommended for proper ripening of most mango cultivars, they were obviously insufficient for cv. 'Tommy Atkins', which shows optimal ripening in the range of 22−32 °C (*29*). Moreover, mature-green fruits are usually subjected to cold storage immediately after harvest to retard ripening during the transport to export markets. However, prolonged cold storage at temperatures below 15 °C may affect the sensory quality and physicochemical characteristics of the fruits when fully ripe (*30*). Additionally, physiological fruit maturity at harvest, which is not known with certainty in this study, also affects the quality of the ripe fruit through the initial status of endogenous ethylene evolution (*31*).

In accordance with the faint β-carotene accumulation, mango fruit ripening resulted in poor pigmentation of the chromoplasts, but in a relevant decline of the starch content, tissue softening, and a significant increase in the sugar/acid ratio. Due to the abundance of pigment-carrying plastoglobuli observed in the chromoplasts irrespective of the ripening stage, an earlier differentiation of chloroplasts into chromoplasts was assumed. Nevertheless, the coexistence of amyloplast and chromoplast plastid types (**Figure 4**) and the remnants of stroma thylakoid structures within the chromoplasts (**Figure 7**) as well as the presence of proplastid-like prolamellar bodies (**Figure 8**) revealed a very dynamic interconversion of the plastid structures in the mango mesocarp tissue, where no sequential pattern could be clearly established. The development of chromoplasts from proplastids, without passing through the chloroplast formation stage, may also occur, as suggested for mutant tomatoes (*8*). These findings contrasted with a study performed on *Arum italicum* Miller, where the plastidial types followed a clear sequence from amyloplasts through chloroplasts to chromoplasts during ripening and presented a pigment profile corresponding to the plastid type observed at each ripening stage (*3*).

The carotenoid profile of mango fruits was established by earlier studies revealing the presence of various isomers of β-cryptoxanthin, luteoxanthin, neoxanthin, violaxanthin (*32*, *33*), and β-carotene (*1*, *15*), even at early ripening stages. The occurrence of carotenoid isomers appears to be linked with a *cis*-isomeric pathway that leads to *cis*-neoxanthin through *cis*-β-carotene and probably exists in parallel to the usual all-*trans* pathways (*3*). Contrarily, isomerization of β-carotene in *Dunaliella salina* algae was found to take place during or after cyclization and to be alternatively light-mediated in the plastid globules (*34*). However, because our previous work established that the portions of *cis*-β-carotene isomers were constant throughout the ripening process of mango fruits, irrespective of light exposure (*1*), other factors enhancing *trans*−*cis* isomerization must be considered. Consistently, β-carotene underwent large changes in its isomeric composition during its accumulation in the globules of green algae cultivated under low illumination conditions (*34*). Furthermore, the same study suggested that β-carotene isomers reflect the changes that occur upon accumulation of globular rather than thylakoidal β-carotene in *D. salina*. The latter indicated that the nature of the structures where the carotenoids accumulate plays a decisive role as to the stability of all-*trans* configurations.

The present study confirmed that carotenoids were mainly deposited in the plastoglobular substructures of the mango chromoplasts. Apparently, plastoglobuli are formed due to lipid overproduction, whereas membranous structures are induced by a higher portion of proteins (*35*). Although it has been established that plastoglobuli are composed of a neutral lipid core surrounded by a monolayer of galactolipids, the exact composition and function of plastoglobuli are unknown and vary between chromoplasts and chloroplasts (*36*). However, it is accepted that lipid molecules may solubilize lipophilic substrates and maintain the stereospecific position of the enzymes involved in carotenoid biosynthesis (*6*). A model describing a membrane-associated enzyme complex for the biosynthesis of carotenoids was proposed (*37*), where the relevance of a lipophilic medium to activate the enzyme systems was indicated. Apparently, carotenoids are synthesized only in lipoprotein membrane structures and further accumulated in the plastoblobuli, where isomerization reactions eventually take place. The latter could be confirmed in this study by the observation that overaccumulation of carotenoids increased the thickness of the membranes, inducing the formation of vesicles (**Figure 6**, see arrows), which then separate from the membrane to form plastoglobuli. Concordantly, due to their similar protein and fatty

acid compositions, it was suggested that plastoglobuli originate from the thylakoids (*36*). Finally, it could be concluded that the accumulation of β-carotene *cis* isomers in the mango chromoplasts is related to the affinity of β-carotene to a lipophilic medium, which is provided by the plastoglobuli.

Unlike mango chromoplasts, carotenoid crystals were predominant in carrot roots (**Figures 10** and **11**). Although carrot chromoplasts consist of pure carotene inclusions (*9*), it should be noted that plastoglobuli were also detected in carrot root chromoplasts, which may carry a minor amount of *cis* isomers. Accordingly, lipid droplets have been observed in ultrastructural studies of carrot roots (*10*). Because the main carotenes, namely, α- and β-carotene, are deposited in their *trans* configurations, it is assumed that the crystalline structure is responsible for the carotene stability. The latter is supported by the *trans*−*cis* isomerization of β-carotene observed in carrot roots subjected to heat treatments, as a result of the disorganization of the crystalline structures and sequestration of the released carotenoid molecules by cellular lipid droplets (*12*).

ACKNOWLEDGMENT

We thank B. Rassow for technical assistance in transmission electron microscopy, as well as K. Mix, B. Jöns, and S. Schilling for assistance in performing the physicochemical analyses.

LITERATURE CITED

(1) Vásquez-Caicedo, A. L.; Sruamsiri, P.; Carle, R.; Neidhart, S. Accumulation of all-*trans*-β-carotene and its 9-*cis* and 13-*cis* stereoisomers during postharvest ripening of nine Thai mango cultivars. *J. Agric. Food Chem.* **2005**, *53*, 4827−4835.

(2) Singh, R. N. *Mango*, 2nd ed.; Indian Council of Agricultural Research: New Delhi, India, 1990.

(3) Bonora, A.; Pancaldi, S.; Gualandri, R.; Fasulo, M. P. Carotenoid and ultrastructure variations in plastids of *Arum italicum* Miller fruit during maturation and ripening. *J. Exp. Bot.* **2000**, *51*, 873−884.

(4) Vásquez-Caicedo, A. L.; Neidhart, S.; Carle, R. Postharvest ripening behavior of nine Thai mango cultivars and their suitability for industrial applications. *Acta Hortic.* **2004**, *645*, 617−625.

(5) Camara, B.; Hugueney, P.; Bouvier, F.; Kuntz, M. Biochemistry and molecular biology of chromoplast development. In *International Review of Cytology*; Jeon, K. W., Jarvik, J., Eds.; Academic Press: New York, 1995; pp 175−247.

(6) Camara, B.; Brangeon, J. Carotenoid metabolism during chloroplast to chromoplast transformation in *Capsicum annuum* fruit. *Planta* **1981**, *151*, 359−364.

(7) Vishnevetsky, M.; Ovadis, M.; Zuker, A.; Vainstein, A. Molecular mechanisms underlying carotenogenesis in the chromoplast: multilevel regulation of carotenoid-associated genes. *Plant J.* **1999**, *20*, 423−431.

(8) Cheung, A. Y.; McNellis, T.; Piekos, B. Maintenance of chloroplast components during chromoplast differentiation in the tomato mutant green flesh. *Plant Physiol.* **1993**, *101*, 1223−1229.

(9) Sitte, P.; Falk, H.; Liedvogel, B. Chromoplasts. In *Pigments in Plants*, 2nd ed.; Czygan, F.-C., Ed.; Gustav Fischer Verlag: Stuttgart, Germany, 1980; pp 117−148.

(10) Frey-Wyssling, A.; Schwegler, F. Ultrastructure of the chromoplasts in the carrot root. *J. Ultrastruct. Res.* **1965**, *13*, 543−559.

(11) Harris, W. M.; Spurr, A. R. Chromoplasts of tomato fruits. II. The red tomato. *Am. J. Bot.* **1969**, *56*, 380−389.

(12) Marx, M.; Stuparić, M.; Schieber, A.; Carle, R. Effects of thermal processing on *trans*-*cis*-isomerization of β-carotene in carrot juices and carotene-containing preparations. *Food Chem.* **2003**, *83*, 609−617.

(13) Lessin, W. J.; Catigani, G. L.; Schwartz, S. J. Quantification of *cis*−*trans* isomers of provitamin A carotenoids in fresh and processed fruits and vegetables. *J. Agric. Food Chem.* **1997**, *45*, 3728−3732.

(14) Castenmiller, J. J. M.; West, C. E. Bioavailability and bioconversion of carotenoids. *Annu. Rev. Nutr.* **1998**, *18*, 19−38.

(15) Pott, I.; Marx, M.; Neidhart, S.; Mühlbauer, W.; Carle, R. Quantitative determination of β-carotene stereoisomers in fresh, dried, and solar-dried mangoes (*Mangifera indica* L.). *J. Agric. Food Chem.* **2003**, *51*, 4527−4531.

(16) International Federation of Fruit Juice Producers (IFU) *Methods of Analysis*; Swiss Fruit Association: Zug, Switzerland, 2001.

(17) Mahayothee, B. *The Influence of Raw Material on the Quality of Dried Mango Slices (Mangifera indica L.) with Special Reference to Postharvest Ripening*; Carle, R., Ed.; Schriftenreihe des Lehrstuhls Lebensmittel pflanzlicher Herkunft, Universität Hohenheim; Shaker Verlag: Aachen, Germany, 2005; Vol. 2.

(18) Marx, M.; Schieber, A.; Carle, R. Quantitative determination of carotene stereoisomers in carrot juices and vitamin supplemented (ATBC) drinks. *Food Chem.* **2000**, *70*, 403−408.

(19) FAO/WHO. *Requirements of Vitamin A, Iron, Folate and Vitamin B12*; FAO Food and Nutrition Series 23; Food and Agriculture Organization of the United Nations: Rome, Italy, 1988.

(20) Zechmeister, L. *Cis*−*trans-Isomeric Carotenoids, Vitamin A and Arylpolyenes*; Springer-Verlag: Wien, Austria, 1962.

(21) Food and Nutrition Board, Institute of Medicine (IOM). *Dietary Reference Intakes for Vitamin A, Vitamin K, Arsenic, Boron, Chromium, Copper, Iodine, Iron, Manganese, Molybdenum, Nickel, Silicon, Vanadium, and Zinc*; a report of the Panel on Micronutrients, Subcommittees on Upper Reference Levels of Nutrients and of Interpretation and Use of Dietary Reference Intakes, and the Standing Committee on the Scientific Evaluation of Dietary Reference Intakes; National Academy Press: Washington, DC, 2002.

(22) van Lieshout, M.; West, C. E.; van Breemen, R. B. Isotopic tracer techniques for studying the bioavailability and bioefficacy of dietary carotenoids, particularly β-carotene in humans, a review. *Am. J. Clin. Nutr.* **2003**, *77*, 12−28.

(23) Tang, G.; Qin, J.; Dolnikowski, G. G.; Russell, R. M.; Grusak, M. A. Spinach or carrots can supply significant amounts of vitamin A as assessed by feeding with intrinsically deuterated vegetables. *Am. J. Clin. Nutr.* **2005**, *82*, 821−828.

(24) Godoy, H. T.; Rodriguez-Amaya, D. B. Occurrence of *cis*-isomers of provitamin A in Brazilian fruits. *J. Agric. Food Chem.* **1994**, *42*, 1306−1313.

(25) Scholz, E. *Karl-Fischer-Titration, Methoden zur Wasserbestimmung*; Springer-Verlag: Berlin, Germany, 1984; pp 15−17, 23−24.

(26) Ruzin, S. E. *Plant Microtechnique and Microscopy*; Oxford University Press: New York, 1999; pp 154−155.

(27) Mahayothee, B.; Mühlbauer, W.; Neidhart, S.; Carle, R. Influence of postharvest ripening processes on appropriate maturity for drying mangoes 'Nam Dokmai' and 'Kaew'. *Acta Hortic.* **2004**, *645*, 241−248.

(28) Schulz, H. Physiologie der lagernden Frucht. In *Physiologische Grundlagen des Obstbaues*; Friedrich, G., Fischer, M., Eds.; Eugen Ulmer Verlag: Stuttgart, Germany, 2000; pp 372−397.

(29) Galán Saúco, V. Recolección y postrecolección. In *El Cultivo del Mango*; Ediciones Mundi-Prensa: Madrid, Spain, 1999; pp 267−291.

(30) Chaplin, G. R.; McBride, R. L.; Abdullah, A.; Nuevo, P. A. Sensory and physico-chemical quality of 'Kensington' mangoes after storage at low temperature. *ASEAN Food J.* **1991**, *6*, 109−113.

(31) Lalel, H. J. D.; Singh, Z.; Tan, S. C. Maturity stage at harvest affects fruit ripening, quality and biosynthesis of aroma volatile compounds in 'Kensington Pride' mango. *J. Hortic. Sci. Biotechnol.* **2003**, *78*, 225−233.

(32) Mercadante, A. Z.; Rodriguez-Amaya, D. B. Effects of ripening, cultivar differences, and processing on the carotenoid composition of mango. *J. Agric. Food Chem.* **1998**, *46*, 128−130.

(33) Pott, I.; Breithaupt, D. E.; Carle, R. Detection of unusual carotenoid esters in fresh mango (*Mangifera indica* L. cv. 'Kent'). *Phytochemistry* **2003**, *64*, 825−829.

(34) Orset, S. C.; Young, A. J. Exposure to low irradiances favors the synthesis of 9-*cis*-β,β-carotene in *Dunaliella salina* (Teod.). *Plant Physiol.* **2000**, *122*, 609−617.

(35) Deruère, J.; Römer, S.; d'Harlingue, A.; Backhaus, R. A.; Kuntz, M.; Camara, B. Fibril assembly and carotenoid overaccumulation in chromoplasts: a model for supramolecular lipoprotein structures. *Plant Cell* **1994**, *6*, 119−133.

(36) Smith, M. D.; Licatalosi, D. D.; Thompson, J. E. Co-association of cytochrome *f* catabolites and plastid-lipid associated protein with chloroplast lipid particles. *Plant Physiol.* **2000**, *124*, 211−221.

(37) Britton, G. Overview of carotenoid biosynthesis. In *Carotenoids: Biosynthesis and Metabolism*; Britton, G., Liaaen-Jensen, S., Pfander, H., Eds.; Birkhäuser Verlag: Basel, Switzerland, 1998; pp 13−147.

Received for review March 16, 2006. Revised manuscript received May 16, 2006. Accepted May 23, 2006. This research was funded by Deutsche Forschungsgemeinschaft (DFG), Bonn, Germany: Project SFB 564-E2. It is part of the Special Research Program 'Research for Sustainable Land Use and Rural Development in Mountainous Regions of Southeast Asia' (Uplands Program).

JF060747U